Nonlinear dynamics of flame fronts with large-scale stabilizing effects

Basile Radisson, Bruno Denet, and Christophe Almarcha
Aix Marseille Université, Centre National de la Recherche Scientifique, Centrale Marseille, IRPHE UMR 7342, 13384 Marseille, France

(Received 31 January 2021; accepted 15 April 2021; published 11 June 2021)

We investigate the influence of gravity and heat loss on the long-time nonlinear dynamics of premixed flames. We show that even when their influence remains weak in the linear regime they can significantly modify the long-time behavior. We suggest that the presence of such a large-scale stabilizing effect could be responsible for the creation of new cells on the front and the appearance of the strong persistent patterns observed in several recent experimental and numerical studies. It could also explain some statistical anomalies observed in the topology of flame fronts.

DOI: 10.1103/PhysRevE.103.063104

I. INTRODUCTION

The propagation of a flame front is often accompanied by the development of instabilities. The primary destabilizing effect [Darrieus-Landau (DL)] is modulated by additional effects (thermal and molecular diffusion within the flame, gravity, heat losses, etc.) and nonlinearities. The interplay between these diverse mechanisms is responsible for permanent fluctuations of the flame front area. This results in fluctuations of the total burning rate and generates variations of propagation speed and pressure in the combustion chamber. These pressure fluctuations are then likely to excite acoustic modes of the combustion chamber. A detailed understanding of the mechanisms involved in the unsteady propagation of flame fronts implies a rigorous understanding of the intrinsic instabilities associated with flame front propagation in both the linear and nonlinear regime.

Over the last decades, several seminal studies carrying out asymptotic analysis have provided a good understanding of flame instabilities in the linear regime. In particular, the specific role played by each effect has been identified: DL [1,2], molecular and mass diffusion [3–7], gravity [3,5,8], viscosity of the gases [5,6], thermal losses [9], and regularization of the flow at finite distance [10].

However, at larger time of propagation, nonlinear effects come into play and have a leading role in the front dynamics. Due to the impossibility of linearizing the governing equations, theoretical analysis of this regime is way more challenging and the understanding of the role played by each effect remains limited compared to the linear regime. From a theoretical standpoint, the major improvements in the comprehension of the nonlinear dynamics of flame fronts have been made through asymptotic analysis either in the limit of small front amplitude ($\epsilon \to 0$) [11–13], with the on-shell description of flame fronts [14,15], or in the limit of small gas expansion through the flame [$\gamma = (\rho_1 - \rho_2)/\rho_1 \to 0$] [16–18]. The latter type of analysis leads to the obtention of the weakly nonlinear Michelson-Sivashinsky (MS) equation:

$$\phi_t + \frac{u_A}{2}\phi_x^2 = \frac{4\sigma_M}{k_c}\left(\frac{\phi_{xx}}{k_c} + I(\phi, x)\right), \tag{1}$$

where ϕ is the local vertical coordinate of the flame front, x is the abscissa, and u_A is a speed that depends on the laminar flame speed and on the density contrast before and after the flame. σ_M is the growth rate of the most amplified wavelength. k_c is the cutoff wave number for which the disturbance amplification due to the Darrieus-Landau effect and the damping due to transport into the thickness of the flames cancel out. $I(\phi, x)$ is a linear operator corresponding to multiplication by $|k|$ in Fourier space. In (1), the second term in the left hand side describes the nonlinear geometrical effect due to the normal propagation of the front, while the right hand side corresponds to the standard dispersion relation for flames when only DL effects and Markstein effects (relaxation by mass and heat diffusion) are considered. Although additional thermodiffusive instability, arising for some particular reactive mixtures, could be investigated and would lead to different equations and nonlinear dynamics [19,20], we focus on the MS equation that has been shown to reproduce qualitatively the essential features observed in usual real flame propagation, especially lean and stoichiometric hydrocarbon-air flames [21–24]. The dynamics described by the MS equation was even successfully compared to direct numerical simulation results [18] and experiments [25,26] on a quantitative level for moderate time of propagation ($\approx 10 \times 1/\sigma_M$). At larger time, we have argued in a recent study that the background noise and sensitivity to initial conditions play an important role in the observed dynamics, therefore limiting a face to face comparison between experiments and numerical simulations [27]. However, we have suggested that the MS equation could still be relevant in predicting some statistical features of the flame front topology. More precisely, we have been interested in the distribution of cell sizes along the front and have been able to predict a theoretical distribution, assuming random splitting on the flame interface. This predicted distribution was shown to compare favorably well with the one observed in numerical integration of the MS equation. It also compared favorably well with the one observed in experiments for hydrocarbon-air flames propagating in a Hele-Shaw burner, except for very large scale. This meant that the experimental large cells are more prone to split in two. To explain this feature, we consider

here additional external mechanisms, present in experiments, and not taken into account in the MS equation. These mechanisms, that could induce the excessive tendency to break for large cells, are considered in this paper. More specifically, we explore, in the late time nonlinear regime, the influence of a large-scale stabilizing effect in the linear regime. As it is well known, gravity effects are stabilizing, especially for large-scale perturbations, in the case of downward propagating flames [13,28]. Furthermore, heat losses, that are enhanced in Hele-Shaw cells with small gap, are known to lead to another type of stabilizing term at large scale [9]. We demonstrate here that these effects, which are damping the linear instability, lead to enhancement of cell splitting in the late time nonlinear regime.

In Sec. II, we therefore first review the different stabilizing effects acting at large scales and we recall their specific influence in the linear regime. From this review, in Sec. III we extract the general component introduced in the dispersion relation by this kind of effect and use a modified MS equation (already proposed by other authors in a different context [22,29–32]) with an additional term expected to mimic these large-scale stabilizing effects. We then compare the dynamics described by this equation with propane-air flames propagating in a Hele-Shaw cell and use these comparisons to suggest that this large-scale stabilizing effect could indeed be responsible for the intriguing features observed experimentally in the nonlinear regime of propagation.

II. LARGE-SCALE EFFECTS ON LINEAR STABILITY

Several external effects acting specifically at large wavelengths have been shown to weaken the classical Darrieus-Landau instability. The purpose of this section is to review these different mechanisms and recall the modification of the classical dispersion relation of flame fronts they imply. Three large-scale effects are reviewed here, pressure gradient induced by gravity [3], cooling length induced by thermal losses [9], and regularization length induced by a flow boundary condition [10]. As the influence of these different effects is more important for small wave numbers, the wavelengths of the perturbations (Λ) considered in this section are large compared with the flame thickness (d_L), allowing us, in this first section, to neglect the modification of the flame structure induced by a wrinkle of the front. The latter will be considered later in this paper.

The standard dispersion relation for the Darrieus-Landau instability is classically obtained from the linear stability analysis of a flame front separating a flow of fresh gases with density ρ_1 and a flow of burnt gases with density ρ_2 (both flows are inviscid and incompressible) and propagating everywhere normally to itself towards the fresh gases with the laminar velocity u_L. The analysis of this problem leads to the standard second order equation [1,2,28]:

$$(2-\gamma)\sigma^2 + 2|k|u_L\sigma - \frac{\gamma}{1-\gamma}u_L^2k^2 = 0 \tag{2}$$

where k and σ are, respectively, the wave number and the growth rate of the considered perturbation and $\gamma = (\rho_1 - \rho_2)/\rho_1$ is the density contrast. This equation admits two real roots. The first one is negative and corresponds to a damped mode. Despite being theoretically predicted by Darrieus and Landau, this damped mode was measured from numerical simulation and compared to the theoretical value, for the first time, only recently [33]. The other root is positive and of the form

$$\sigma = \Omega u_L|k| \tag{3}$$

where Ω is a function of γ (e.g., see [28] for the expression of Ω). In the limit where the considered wavelength is large compared to the flame thickness and diffusion effects in the thickness of the flame can be neglected, Eq. (3) predicts that any perturbation of the flame front will grow exponentially with a growth rate inversely proportional to the wavelength of the perturbation.

A. Gravity effect

When gravity is introduced in the problem (note that we do not present here the dispersion relation in the limit of very small Hele-Shaw cell thickness, which can be found in [8]), the dispersion relation (2) becomes

$$(2-\gamma)\sigma^2 + 2ku_L\sigma - \gamma k\left(\frac{u_L^2k}{1-\gamma} + g\right) = 0 \tag{4}$$

where the gravity g is oriented perpendicularly to the unperturbed front and considered positive when directed toward the burnt gases. Equation (4) admits a positive root in the form

$$\sigma = \frac{1}{2(2-\gamma)}\left[\sqrt{4k^2U_L^2+4(2-\gamma)\gamma\left(\frac{U_L^2k^2}{1-\gamma}+kg\right)}-2kU_L\right] \tag{5}$$

which reduces to the classical DL growth rate (3) when $g = 0$.

The growth rate given by (5) is plotted on Fig. 1(a) for different values of g. As it is shown, in the case of an upward propagating flame ($g > 0$), the DL instability is enhanced by gravity effects. On the other hand, when the flame is propagating downward, the DL instability is inhibited. In both cases, the relative variation of growth rate with gravity is larger for long wavelengths. Indeed, in relation (4), the importance of g is increased compared to u_L^2k when k is small.

B. Thermal losses

The influence of thermal losses on the stability of flame fronts was studied by Joulin and Sivashinsky [9]. Their analysis leads to an expression (obtained only in the small γ limit) for the growth rate of a perturbation, accounting for the effect of viscous (characterized by a friction coefficient ζ) and thermal dissipation (characterized by a heat loss coefficient χ). Here, we consider the Joulin and Sivashinsky expression in the limit $\zeta \to 0$ and $g \to 0$:

$$\sigma = \frac{\gamma u_L|k|}{2}\left(\frac{\rho_1 u_L|k|}{\rho_1 u_L|k| + \chi/C_P}\right). \tag{6}$$

This growth rate expression is plotted on Fig. 1(b) for different values of the thermal losses parameter χ. As we can see, the role of thermal losses is to damp the Darrieus-Landau growth rate, particularly for the small k. Indeed, the thermal losses introduce a cooling length l_χ in the problem which

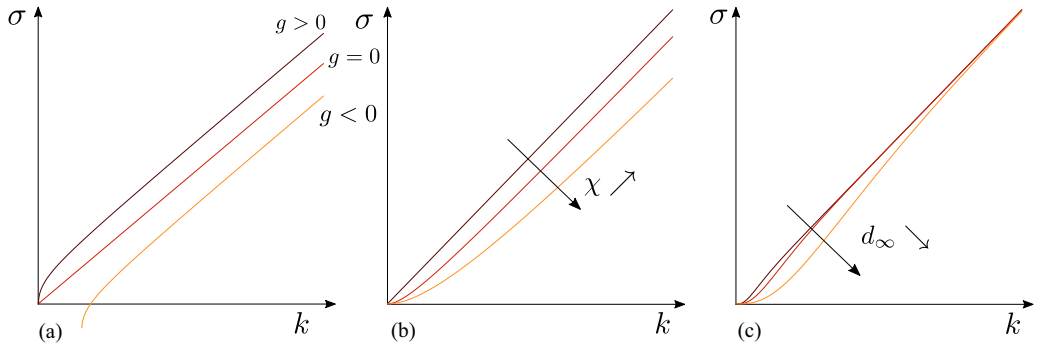

FIG. 1. Modification of the DL dispersion relation by different large-scale effects. (a) Effect of gravity: for upward (respectively downward) propagating flames the instability is enhanced (respectively inhibited), particularly for small k. (b) Effect of thermal losses: when the thermal losses coefficient χ is increased, the instability is damped particularly on large scales. (c) Effect of a flow boundary condition at finite distance d_{reg} of the front.

corresponds to the typical distance behind the flame over which the burnt gases are cooled down to the initial fresh gases temperature. As a typical perturbation of the front is associated with a perturbation of the flow decreasing on a length $l_r \sim \exp(-k|Y|)$ [28] on both sides of the flame, the considered perturbation will be slightly affected if $l_r \ll l_\chi$. On the other hand, if $l_r \gg l_\chi$ the perturbation will almost not see the density contrast through the flame, which will damp the DL instability for small k. The influence of thermal losses is thus similar to the stabilizing effect of gravity on downward propagating flames, as it regularizes the long wavelength perturbations.

C. Flow regularization at finite distance

The presence of a flow boundary condition, at finite distance ahead of the flame, is also prone to disturb the flame dynamics. The problem has been first analyzed analytically by Joulin [10] in the framework of a flame stabilized near a porous flat burner inlet. He demonstrated that the DL effect is weaker than in an unbounded flow. The difference relies in the boundary condition which imposes the flow regularization. In the classical DL problem, the flow is regularized at $Y = \pm\infty$ ahead and behind the flame front. Here, due to a prescribed mixture inlet at finite distance $Y = -d_{\text{reg}}$, the boundary condition for the perturbation of the flow speed $u'(Y_{\text{bound}}) \sim v'(Y_{\text{bound}}) = 0$ is translated from $Y = -\infty$ to $-d_{\text{reg}}$. Performing the linear stability analysis with this new boundary condition, Joulin [10] found a modified DL dispersion relation. Here, for brevity, we present only the obtained expression for the growth rate $\sigma(k)$ in the $\gamma \to 0$ limit (the reader is directed towards Joulin's paper for the finite γ case):

$$\sigma = \Omega_{sg} u_L |k| [1 - \exp(-|k| d_{\text{reg}})]^2 \tag{7}$$

where Ω_{sg} is the asymptotic value of Ω when $\gamma \to 0$. This expression reduces to (3), when the distance of the regularizing boundary condition d_{reg} tends to ∞. The expression of $\sigma(k)$ given by (7) is plotted on Fig. 1(c). The smaller the d_{reg}, the weaker the DL growth rate. As with gravity and thermal losses, and for the same reason, large scales are more affected.

The initial purpose of Joulin's study was to understand the reason for flame stabilization near a flat burner. Actually, the impact of its result can be extended to the more general case of a flow regularized at finite distance of the flame front. For example, considering direct numerical simulation for flame dynamics study [34–39], the numerical domain in the Y direction must be very large compared to the considered wavelengths. If not, the prescribed boundary conditions at the inlet and outlet of the domain may modify the standard Darrieus-Landau picture. In addition, and particularly for no-slip boundary conditions, the growth rate could also depend on the width of the numerical domain in the x direction.

To conclude, the three effects reviewed here are prone to weaken the standard DL growth rate. Their influence is more sensitive on the large scales ($k \to 0$) where a cut-off wavelength $\lambda_g = 2\pi/k_g$ is eventually introduced. This is a significant modification to the standard Darrieus-Landau problem which is devoid of any characteristic length scale.

III. LARGE-SCALE EFFECTS ON NONLINEAR DYNAMICS

A. Modified Michelson-Sivashinsky equation

We want to incorporate the long range stabilizing effects into the integrodifferential MS equation (1) in order to take their influence into account in the late time nonlinear dynamics of the flame. For this purpose the dispersion relation associated with the MS equation is modified in the form

$$\sigma(k) = \frac{4\sigma_M}{k_c}\left(|k| - \frac{k^2}{k_c}\right) + G \tag{8}$$

where G (if negative) is a damping rate associated with one or several of the stabilizing effects reviewed in the previous section. With the rough approximation chosen here, the value of G is the same for all wavelengths. If $G \ll \sigma_M$, this constant damping rate slightly lowers the growth rate for all wavelengths and introduces a additional cut-off wavelength on the left side of the dispersion relation. It is therefore a convenient approximation to mimic the influence of gravity, thermal losses, and/or regularization of the flow at finite distance (see previous section). Moreover, the nonlinear (MS kind) equation associated with (8) can be obtained in a rigorous manner in the framework of a small γ expansion. The methodology to achieve this is the same as the one used to obtain the standard MS equation [16], but taking into account gravity

in the momentum conservation equation. Such an analysis has been first proposed by Rakib and Sivashinsky [40] for the thermodiffusive case. For flames subject to hydrodynamic instability only, the most rigorous development was carried out by Boury [41]. The obtained equation (MSG later in this paper) is of the form

$$\phi_t + \frac{u_A}{2}\left(\phi_x^2 - \langle\phi_x^2\rangle\right) = \frac{4\sigma_M}{k_c}\left(\frac{\phi_{xx}}{k_c} + I(\phi, x)\right) + G(\phi - \langle\phi\rangle) \tag{9}$$

which reduces to (1) in the limit $G \to 0$ through a simple change of frame of reference. Numerical experiments obtained by pseudospectral integration of Eq. (9) report a strongly modified dynamics (even for $G \ll \sigma_M$) compared to the standard MS model [22,29–32]. Simulations of this modified MS equation will be compared to experiments in the rest of the paper. As we shall see, this simple pseudo-differential equation is able to reproduce some interesting features observed in our experiments (and other recent ones [42]). However, as this equation is valid only in the small γ limit, it would be also interesting, in a future work, to simulate the on-shell description of flame fronts, which has been recently extended to a case with gravity [43] for upward propagating flames.

B. Comparison with experiments

The dynamics described by (9) will now be compared to experimental flames. For this purpose, we make use of the Hele-Shaw burner employed in our recent studies [27,33,44,45]. This apparatus is made of two borosilicate glass plates (1500 × 500 × 5 mm) oriented vertically and separated by a 5-mm gap. The burner cavity is opened at the top, and closed on the two vertical sides and at the bottom. For the experiments presented hereafter, the burner is filled with a propane-air mixture $\phi = 0.8$ through a flow line positioned at the bottom of the experimental facility and controlled by two Bronkhorst EL-Flow series mass-flow regulators. Before flame ignition, the flow rate of the mixture is adjusted so that the speed of the flow at the top outlet of the burner is slightly in excess of the flame speed. This technique allows the flame to remain anchored at the top of the burner as an inverted V flame. After ignition of the flame, the mixture flow is then suddenly stopped thanks to a solenoid valve and the flame starts its downwards propagation. In Fig. 3(a) a typical example of the front evolution observed in the burner is shown. Here, the initial shape of the flame (corresponding to the first flame front contour at the top of the figure) was experimentally selected using a laser cut plate positioned at the top of the burner (see [45] for details about this experimental technique). The same experimental technique using plates with a sinusoid shape at the top allows one to force modes of different wavelengths and to measure their growth rates (see [45] for details). Some of these measurements are presented in Fig. 2 and describe the dispersion relation of these experimental flames. These data are then used as an indirect measurement of the parameters σ_M, k_c, and G involved in (9). The procedure to obtain their value is the same as the one employed in [27], but the modified dispersion relation (8) instead of the standard one associated with (1) is fitted on the growth-rate measurements using a

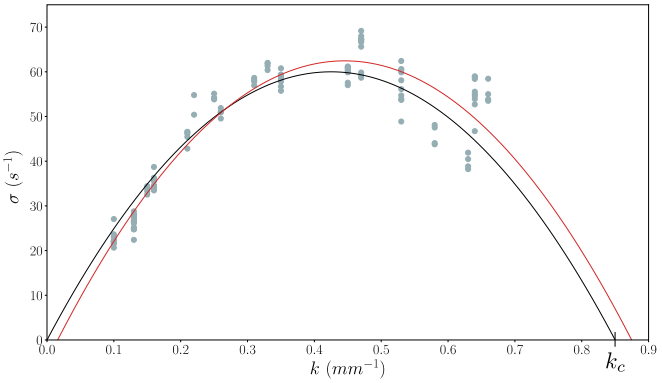

FIG. 2. Growth rate measurements obtained for a propane-air flame $\varphi = 0.8$. The obtained values are then fitted with theoretical expressions for the growth rate. Red line: Fit with the modified dispersion relation (8). Black line: Fit with the same dispersion relation and $G = 0$.

Levenberg-Marquardt algorithm (see Fig. 2). The best set of parameters given by the fitting algorithm is $\sigma_M = 67\ \mathrm{s}^{-1}$, $k_c = 0.89\ \mathrm{mm}^{-1}$, and $G = -4.7\ \mathrm{s}^{-1}$.

As can be seen, the differences between the fit obtained here (red line) and the one obtained in [27] on the same data but with the standard dispersion relation (black line) are small. In particular, the dispersion relation is slightly shifted towards the large wave numbers and a additional cut-off wave number is introduced on the left side of the dispersion relation. In the following, we shall demonstrate that despite this small difference in the linear regime these new ingredients have actually a strong influence on the late time nonlinear dynamics.

For this purpose, a flame front is extracted from the experiment presented in Fig. 3(a) (first flame front at the top). This front is used as an initial condition $\phi(x, t = 0)$ for a direct numerical simulation of Eq. (9). The integration is performed by pseudospectral spatial discretization with periodic boundary conditions. The time derivatives are discretized using first order finite differences (forward and backward Euler). The obtained evolution for the flame front is compared with experiment in Fig. 3. Three different simulations with three different sets of parameters are run with this same initial condition. The first one [Fig. 3(b)] is obtained with parameters corresponding to the black line dispersion relation in Fig. 2. This corresponds to the standard MS equation exploited in [27] ($G = 0$). The second one [Fig. 3(c)] is obtained using the parameters corresponding to the best fit of (4) on our growth rate data (red line on Fig. 2). The last one is obtained by keeping the same σ_M and k_c but adjusting G empirically in order to better match the dynamics observed in the experiment. By comparing the MSG simulations [Figs. 3(c) and 3(d)] with the standard MS one [Fig. 3(b)], we can see that the first mergers are still well reproduced and the top half part of the evolution looks very similar to the one given by standard MS [Fig. 3(b)]. The differences are visible in the second part of the evolution. With standard MS [Fig. 3(b)], the mergers were too fast compared to the experiments. In [27], these differences were assigned to the stochastic process of new crests addition which is not described by a noise free MS dynamics. However, even if these crest appearances are

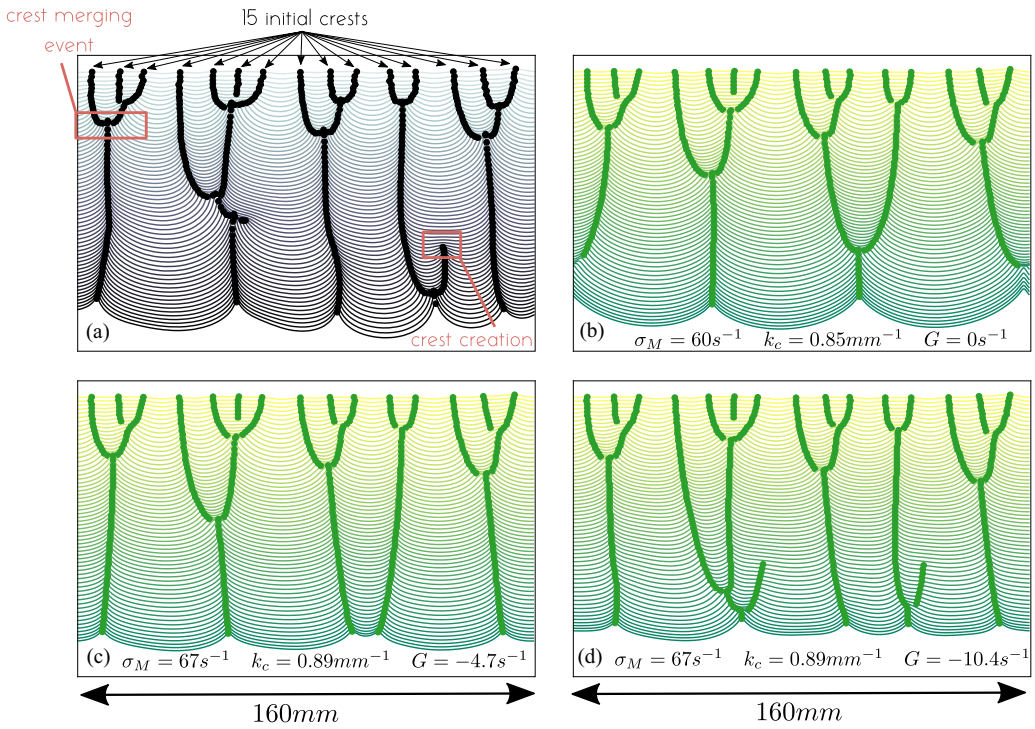

FIG. 3. Comparison of experimental flame (propane-air $\varphi = 0.8$, $u_L \approx 0.3$ m s^{-1}) front evolution with the ones given by MS numerical integration or MSG numerical integration. Each line corresponds to the contour of the flame front at one instant in time with the initial configuration at the top and the final one at the bottom. The positions of the crests are highlighted with dots allowing one to visualize their trajectories. The merging events mentioned in the main text correspond to the instants where two or more crest trajectories collapse on each other. The crest creation events correspond to the sudden appearance of a new trajectory. (a) Typical evolution observed in our experiments. The first flame front at the top is used as an initial condition for MS and MSG numerical integration. (b) MS numerical integration starting from the experimental initial condition. The parameters are $\sigma_M = 60$ s^{-1}, $k_c = 0.85$ mm^{-1}, $G = 0$ s^{-1}. (c) MSG numerical integration with parameters $\sigma_M = 67$ s^{-1}, $k_c = 0.89$ mm^{-1}, $G = -4.7$ s^{-1}. (d) MSG numerical integration with parameters $\sigma_M = 67$ s^{-1}, $k_c = 0.89$ mm^{-1}, $G = -10.4$ s^{-1}.

responsible for the dispersion of crest trajectories between experimental runs (see [27] Fig. 12), one can observe that the new crests are appearing always in the same areas. The latter remark suggests that these crest appearances are not as random as we guessed. Indeed, on MSG simulation [Fig. 3(c)], large cells are flattened and the aggregation process seems to be slower in the second part. It results in a dynamics which agrees with experiment on a time larger than the standard MS dynamics. However, the fitted value of G seems to be too small to perfectly reproduce the evolution in Fig. 3(a). Therefore, we have performed MSG integration for larger values of G. The experimental evolution is nearly perfectly reproduced for a value of $G = -10.4$ s^{-1} [Fig. 3(d)]. The merging process is completely slowed by the large-scale additive term, which results in nearly straight crest trajectories (bold lines on the figure) in the second part of the evolution (as observed in the experiment). However, the two crest creations are well reproduced. Obviously, such an *a posteriori* parametrization is not praiseworthy. But, as highlighted in Sec. II, several mechanisms may be involved in a large-scale cutoff such as the G additional term. Unfortunately, effects such as thermal losses are probably not taken into account by the fit obtained in Fig. 2. Indeed, our growth rate measurements are performed in the very first instants of flame propagation when the flame is near the top of the burner. Therefore, the thermal losses effect induced by walls is probably weaker than when the flame is lower in the burner. At this time, we are still not able to ignite a flat flame lower in the burner. Thus, we have no way to accurately estimate the experimental G value associated with the joint effect of thermal losses and gravity, and we are restricted to a numerical parametric investigation. This is why, in the next section, the influence of G on the long-time behavior is numerically explored.

C. Long-time evolution

Three long-time simulations are performed starting from a noisy flat initial condition. The parameters used correspond to the cases studied in Fig. 3. The first one (see Fig. 4) corresponds to the case studied in Fig. 3(b) but for a domain of width $\Lambda = 500$ mm instead of $\Lambda = 158$ mm. After a short stage of aggregation, the numerical noise is responsible for the appearance of new cells. It results in large-scale patterns with smaller cells living on it. The two other simulations (Figs. 5 and 6) result from longtime integration of the MSG model (9). The parameters used are the same as those used in Figs. 3(c) and 3(d) (respectively), but for a larger domain width ($\Lambda = 500$ mm). The longtime dynamics is completely different from the MS ones. The new crest creations start earlier in the propagation process, resulting in a smaller mean cell size (as identified by Boury *et al.* [32]). Moreover, a particular feature is observed here. The evolution process exhibits

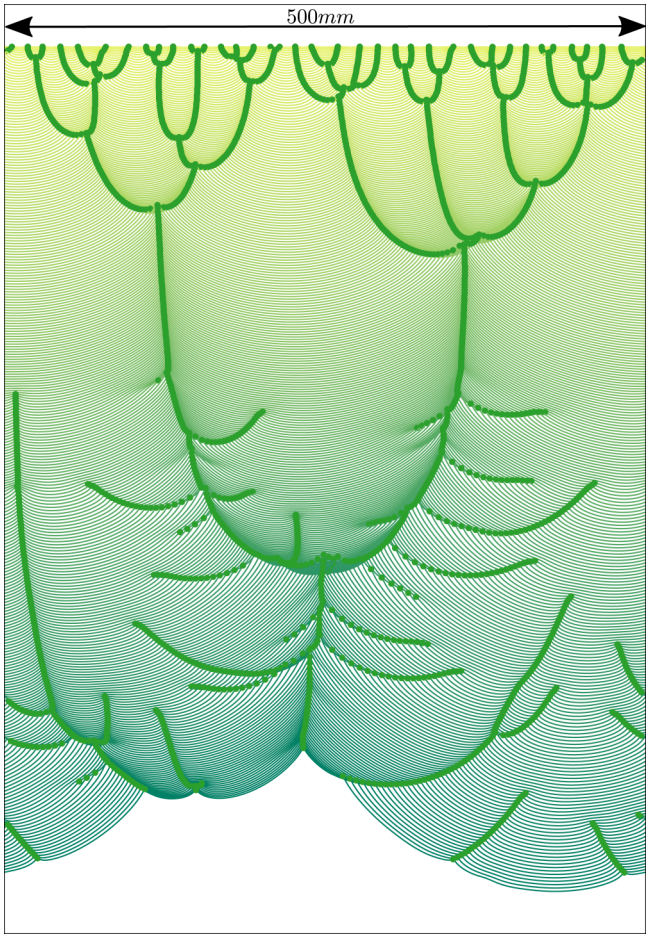

FIG. 4. Numerical integration of the MS model for parameters $\sigma_M = 60\ \mathrm{s}^{-1}$, $k_c = 0.85\ \mathrm{mm}^{-1}$, $\Lambda = 500$ mm. The lateral boundary conditions are periodic. After a purely aggregative stage, the noise is responsible for the addition of new cells. At final stage, the flame front is composed of large-scale structures with smaller ones living on it.

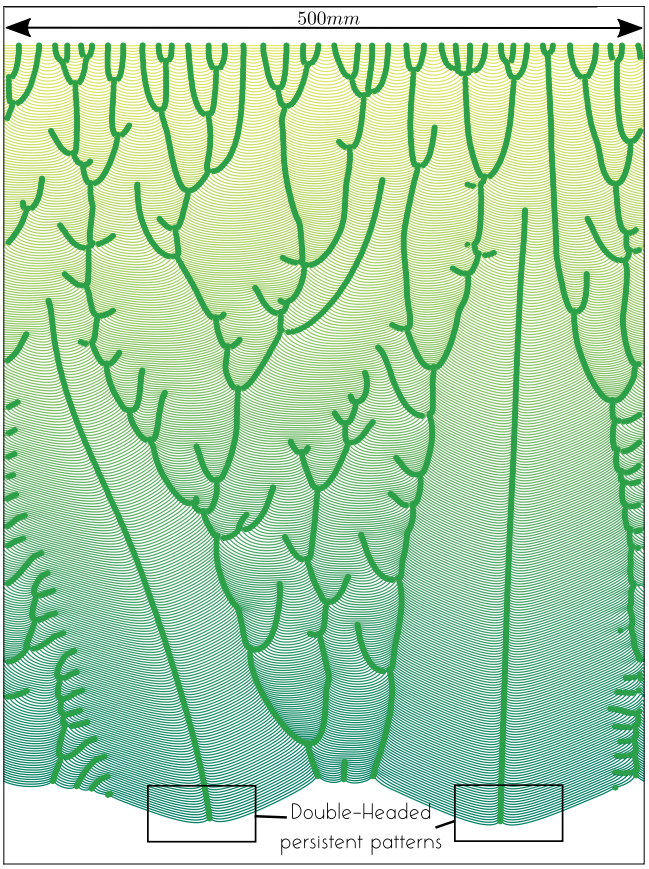

FIG. 5. Numerical integration of the MSG model for parameters $\sigma_M = 67\ \mathrm{s}^{-1}$, $k_c = 0.89\ \mathrm{mm}^{-1}$, $G = -4.7\ \mathrm{s}^{-1}$, and $\Lambda = 500$ mm. The new cell appearance stage appears earlier than for the MS dynamics. On larger time of evolution some large persistent patterns are observed and lead the flame propagation.

strong double-headed persistent patterns leading to the flame propagation. It seems that these arrangements are not only resulting from the G value because it looks weaker in the case $G = -10.4\ \mathrm{s}^{-1}$ than in the case $G = -4.7\ \mathrm{s}^{-1}$. As they persist, these patterns may be responsible for a modification of the cell-size distribution.

D. Modification of the cell-size distribution

The nondimensional cell-size distributions are computed from long-time simulations of the MSG model for the two cases plotted in Figs. 5 and 6. For each of the two sets of parameters, a series of 50 long-time simulations starting from random initial conditions (flat front with a small gaussian white noise added on it) is performed. The time evolution of the cell-size distribution is then computed from the obtained flame front until it reaches a stationary state. The nondimensional stationary cell-size distribution is plotted in Fig. 7. The presence of persistent patterns is clearly visible. The distribution is now bimodal, particularly for $G = -4.7\ \mathrm{s}^{-1}$, where the persistent patterns are clearly larger than the most probable size.

The presence of double-headed persistent patterns has been reported in the literature for thermodiffusively unstable flames [46] and localized flames [47]. Here, we demonstrate that these gravity and heat-loss effects are favorably taken into account in the G parameter for continuous flames, even in the absence of thermodiffusive instability. The leading pattern has probably not been observed before in that condition because all the MSG simulations were focused on small size domain [22,29–31] except for Boury's studies [32,41]. In the latter, however, the MSG integration was stopped as soon as new crests were starting to appear and the long-time dynamics was not studied. From a purely theoretical standpoint, the emergence of persistent patterns is fascinating because this behavior is not possible with the standard MS equation. Indeed, for a periodic domain like the one exploited in the present numerical simulations, it was demonstrated that the only stable configuration is the so-called monocellular conformation [48,49]. This means that the slight modification introduced into the dispersion relation by the addition of the G term in the MSG model is able to break the aggregative process of crests associated with the horizontal attraction between the poles of the analytic solution of the MS equation [50]. The

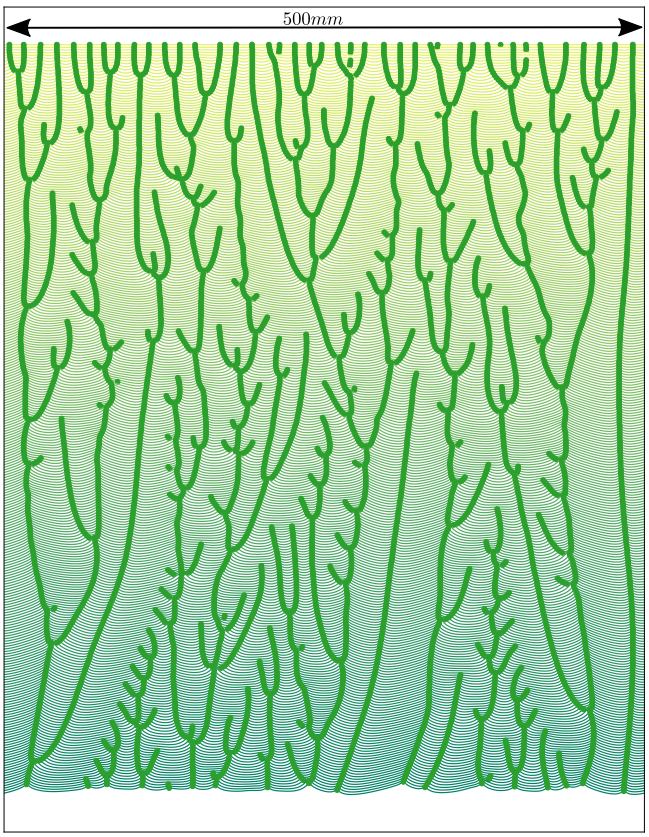

FIG. 6. Numerical integration of the MSG model for parameters $\sigma_M = 67\ \mathrm{s}^{-1}$, $k_c = 0.89\ \mathrm{mm}^{-1}$, $G = -10.4\ \mathrm{s}^{-1}$, and $\Lambda = 500$ mm. The persistent patterns are smaller and weaker than for the previous case.

latter is not really surprising because the MSG equation does not admit pole solutions like the standard MS equation. This means that there is no pole dynamics associated with (9) and therefore a crests aggregation scenario is probably no longer relevant. Indeed, as first identified by [22] (in the context of spherically expanding flames) and Denet [30] (in the context of flat average flame fronts submitted to gravity), G is responsible for the breaking of cells. A stabilizing large-scale effect $G < 0$ has thus a destabilizing influence for the curved nonlinear shape. This new size selection mechanism leads the flame front evolution to a stationary mean cell size $\langle d \rangle$ smaller than the size domain, even in the absence of noise [32,41]. For large domain Λ as shown in Figs. 4–6 the joint effects of numerical noise and G are involved in the cells breakup. The relative magnitude of these two protagonists is probably responsible for the appearance of persistent arrangements.

E. Modification of the flame brush thickness

When increasing the importance of the gravity term, as shown in Fig. 8, the cusps trajectories tend to align with the vertical direction, thus reducing the usual merging or fusion process. In addition, the gravity force inhibits the vertical extension of the flame. This flattening effect can be computed by the flame brush thickness, the distance H between the upper and lower level of the flame, as reproduced in Fig. 9, for parameters $\sigma_M = 67\ \mathrm{s}^{-1}$, $k_c = 0.89\ \mathrm{mm}^{-1}$, $\Lambda = 500$ mm, $u_A = 645\ \mathrm{mm\,s}^{-1}$. The values reported are a mean computed during the late time regime. When increasing the gravity term, the flame brush thickness decreases like $H \approx (-G)^{-3/2}$.

F. About real flames

We want to highlight that these new features are not only interesting from a purely theoretical standpoint. These double-headed patterns are also of practical interest and have been observed in direct numerical simulation carried out on large domains [38] and in recent experiments where they were shown to lead the flame front propagation in unusual regimes [42]. In the following we present some experiments where the G effect is varied and we analyze its influence on the flame front topology.

Here, the G parameter is varied in two ways: first by decreasing the gap between the two plates of the burner, and second by diluting the mixture with nitrogen.

1. Thermal losses influence

By decreasing the gap of the burner from $\Delta = 5$ to 3 mm, the thermal losses are increased (equivalent to a larger G value in the MSG equation). In this configuration, strong persistent

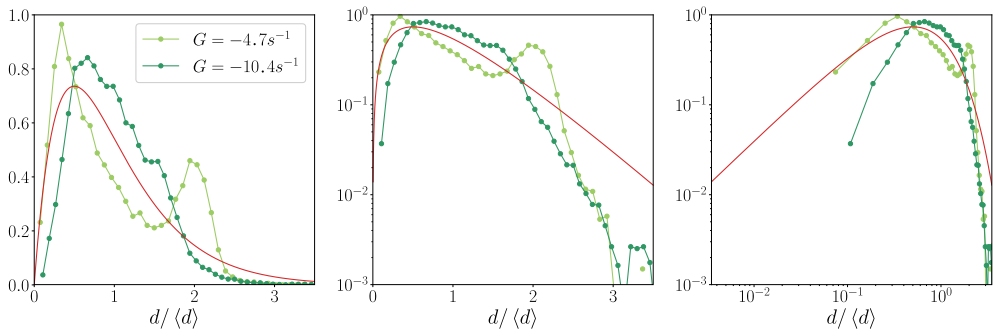

FIG. 7. Cell-size distributions obtained from numerical integration of the MSG model. The simulations are carried out with periodic boundary condition and are initialized with a flat front with a small gaussian white noise added on it. The distribution is bimodal due to the presence of strong persistent patterns larger than the mean cell size. For the case $G = -10.4\ \mathrm{s}^{-1}$ the persistent patterns are smaller and just responsible for an enlargement of the maximum of the distribution. The theoretical gamma distribution $\iota = 2$ is shown (red line) for comparison.

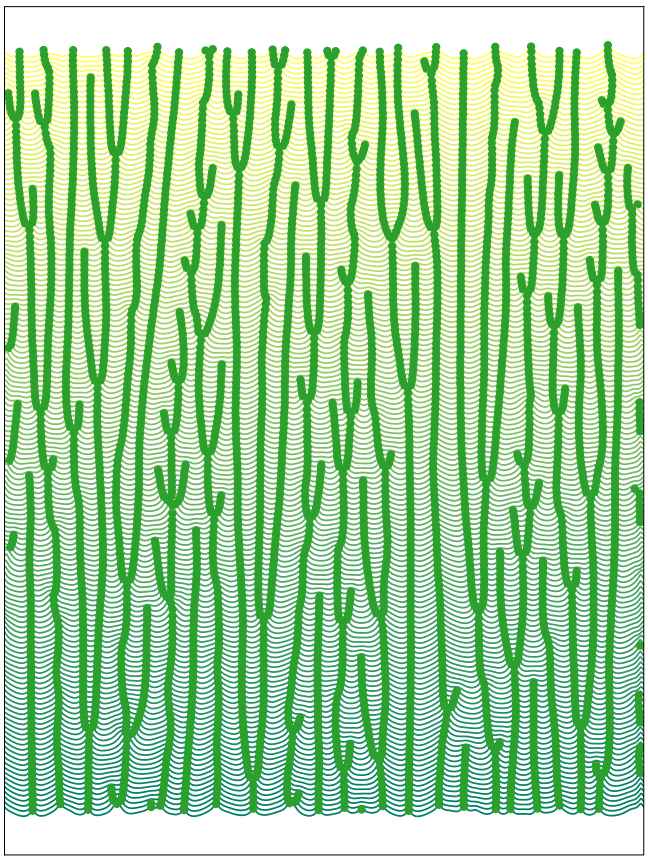

FIG. 8. Numerical integration of the MSG model for parameters $\sigma_M = 67\ \mathrm{s}^{-1}$, $k_c = 0.89\ \mathrm{mm}^{-1}$, $\lambda = 500$ mm, and $G = -20\ \mathrm{s}^{-1}$.

patterns are observed (see Fig. 10). Their influence on the cell-size distribution is visible in Fig. 11, where the bimodal aspect is perceptible.

2. *Froude number effect*

Another way to vary experimentally the G effect is through nitrogen dilution of the reactive mixture. For this purpose, the burner gap is readjusted to $\Delta = 5$ mm, the equivalence ratio is fixed at $\varphi = 1.1$, and the propane-air mixture is diluted with nitrogen for different dilution ratios:

$$\delta = \frac{V_{O_2}}{V_{O_2} + V_{N_2}}. \tag{10}$$

By varying δ, the laminar flame speed is modified, and the relative effect of gravity with respect to the Darrieus-Landau

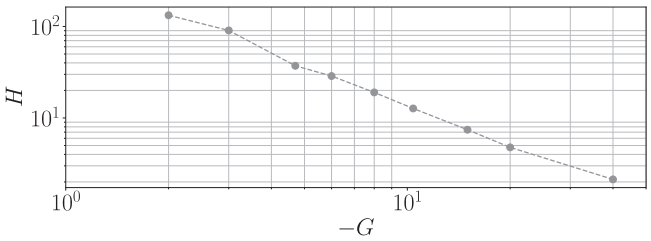

FIG. 9. Decrease of the flame brush thickness H (mm) with increase of the gravity parameter $-G$ (s^{-1}).

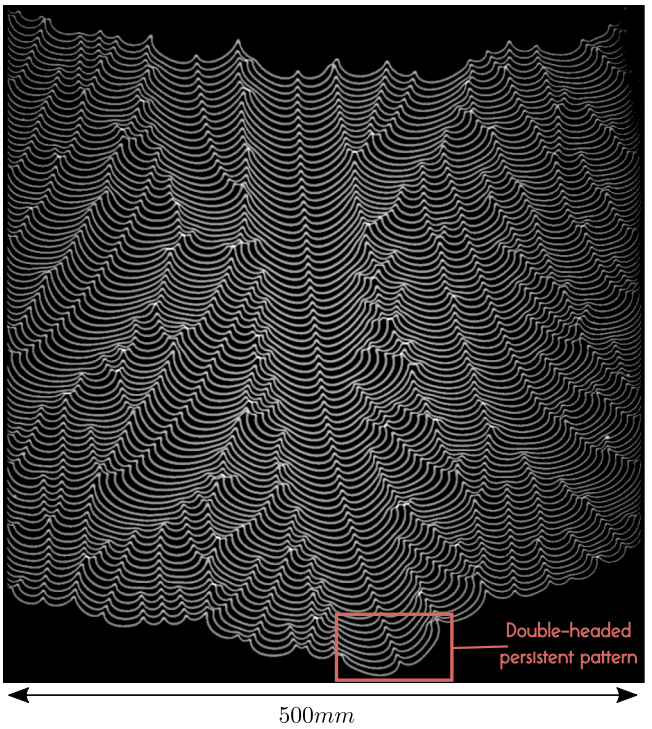

FIG. 10. Propane-air flame ($\varphi = 0.8$, $u_L \approx 0.3\ \mathrm{m\,s}^{-1}$) propagation in a thin Hele-Shaw burner ($\Delta = 3$ mm). Some persistent patterns are clearly visible.

effect is changed. The relative influence of both effects is characterized by the Froude number:

$$\mathrm{Fr} = \frac{u_L}{\sqrt{g d_L}} \tag{11}$$

based on u_L the laminar flame speed, d_L the laminar flame thickness, and g the standard gravity constant. In order to determine the corresponding Froude number for each dilution ratio used in our experiments, we carry out freely propagating flat flame simulations with Cantera [51] using a complex chemical-kinetic San Diego mechanism [52]. The u_L and d_L values are then defined from the velocity and temperature profile given by these simulations by taking u_L as the flame speed relative to the unburnt mixture and d_L as

$$d_L = \frac{T_b - T_u}{\max(dT/dy)} \tag{12}$$

with T_b (respectively T_u) the temperature in the burnt gases (respectively in the unburnt gases). The cell-size distribution, for each dilution ratio, is then computed from a large number of experiments following the procedure described in [27]. The result is plotted in Fig. 12. As with the thermal losses, the cell-size distribution narrows when the gravity effect is increased, moving away from the theoretical gamma distribution. The presence of persistent patterns is less visible in the statistics. Actually, some are clearly observed in the case $\delta = 0.168$ but their typical size is close to the most probable size. It results in an enlargement of the pair distribution function maxima.

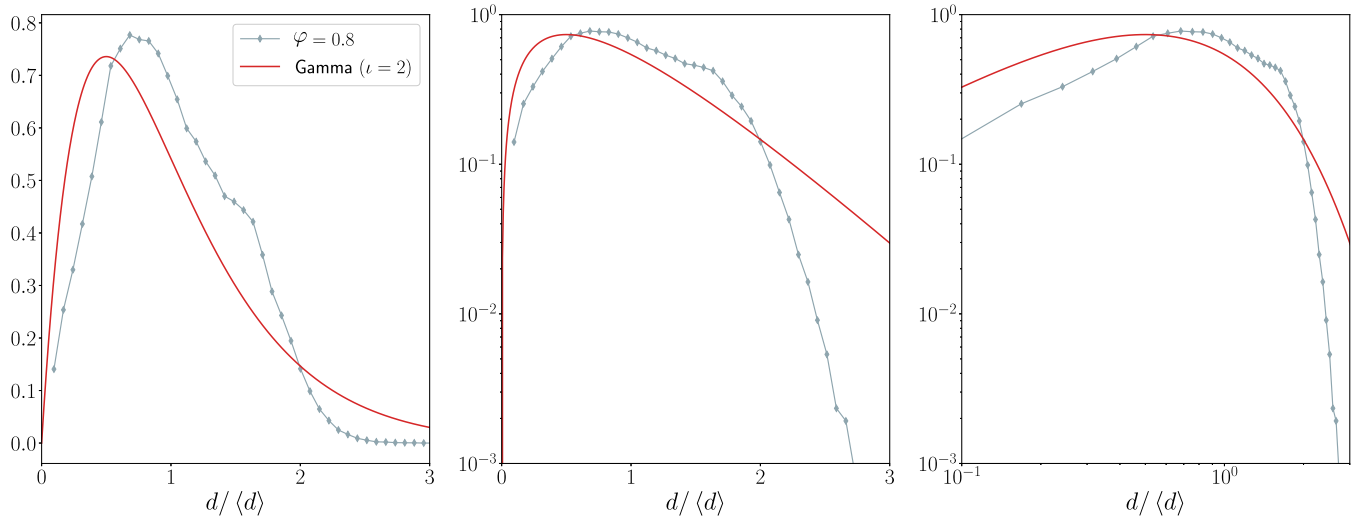

FIG. 11. Cell-size distributions obtained from experiments in a burner with a thinner gap ($\Delta = 3$ mm). The presence of persistent patterns is clearly visible. The theoretical gamma distribution $\iota = 2$ is shown (red line) for comparison.

IV. CONCLUSION

We have observed in this paper that large-scale stabilizing effects, which are naturally present in Hele-Shaw experiments (downward propagating flames, heat losses) are relatively weak in the linear instability regime. Indeed the growth rates of the hydrodynamic instability are not extremely modified by the addition of these terms. However, the situation is completely different in the nonlinear regime, and we have shown that these large-scale stabilizing effects can even qualitatively change the nonlinear dynamics of these flames. It seems that these effects are likely to compete with the aggregative tendency of cells and may explain the preferential splitting highlighted in [27]. Moreover, we report that these effects are responsible for the appearance of strong persistent double-headed arrangement leading the flame as already observed in [26]. The stability of these patterns is not yet understood but it seems that the presence of a large-scale cutoff mechanism and a noise influence are two basic ingredients that are required for their appearance. The leading structures have also been observed (not discussed however) in the large-scale numerical simulations of Yu *et al*. [38]. Although no gravity effect or thermal loss was taken into account in that study, the confinement in the direction normal to the front is probably responsible for a *G*-like effect in this case. Finally, other double-headed flame fronts were recently reported in theoretical [8,46] and experimental [42] studies as a characteristic of subunity Lewis number flames. In these studies, the double head was eventually located on isolated flames [42]. Here, we demonstrated that double-headed leading patterns are not restricted to low Lewis number, provided that a gravity or confinement or heat loss is present and that the domain size is large enough.

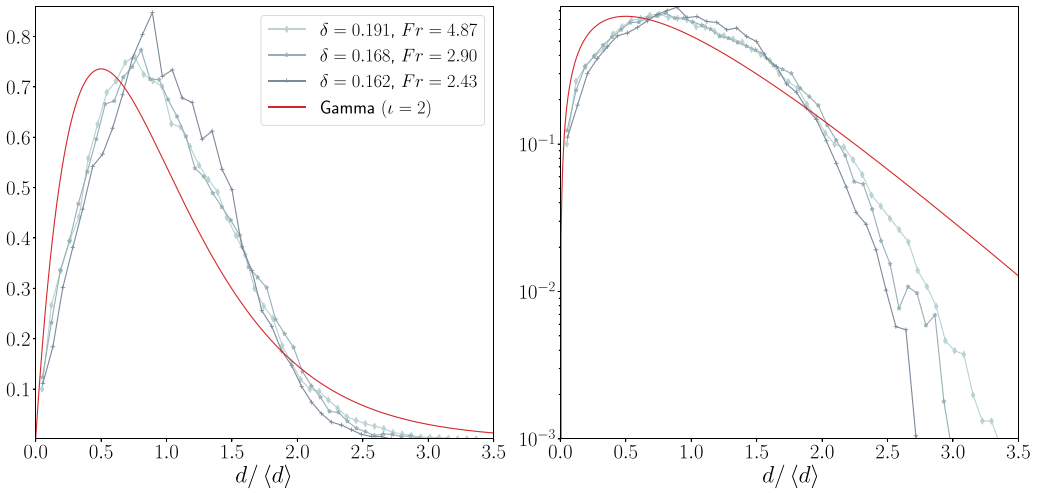

FIG. 12. Experimental cell-size distributions for propane-air flame $\varphi = 1.1$ for different dilution values (corresponding to different Froude numbers). The theoretical gamma distribution $\iota = 2$ is shown (red line) for comparison. Left: lin-lin scale. Right: Same with lin-log scale.

[1] G. Darrieus, Propagation d'un front de flamme, La Technique Moderne **30**, 18 (1938).

[2] L. D. Landau, On the theory of slow combustion, Acta Phys. **19**, 77 (1944).

[3] G. H. Markstein, *Non-Steady Flame Propagation* (Pergamon, New York, 1964).

[4] G. I. Barenblatt, Y. B. Zeldovich, and A. G. Istratov, On heat and diffusion effects in stability of laminar flames, ZhPMTF **4**, 21 (1962).

[5] P. Pelcé and P. Clavin, Influence of hydrodynamics and diffusion upon the stability limits of laminar premixed flames, J. Fluid Mech. **124**, 219 (1982).

[6] M. Matalon and B. J. Matkowsky, Flames as gasdynamic discontinuities, J. Fluid Mech. **124**, 239 (1982).

[7] P. Clavin and P. Garcia, The influence of the temperature dependence of diffusivities on the dynamics, J. Méc. Théor. Appl **2**, 245 (1983).

[8] D. Fernández-Galisteo and V. N. Kurdyumov, Impact of the gravity field on stability of premixed flames propagating between two closely spaced parallel plates, Proc. Combust. Inst. **37**, 1937 (2019).

[9] G. Joulin and G. Sivashinsky, Influence of momentum and heat losses on the large-scale stability of quasi-2D premixed flames, Combust. Sci. Technol. **98**, 11 (1994).

[10] G. Joulin, On the hydrodynamic stability of flat-burner flames, Combust. Sci. Technol. **53**, 315 (1987).

[11] V. V. Bychkov, Nonlinear equation for a curved stationary flame and the flame velocity, Phys. Fluids **10**, 2091 (1998).

[12] V. V. Bychkov and A. Kleev, The nonlinear equation for curved flames applied to the problem of flames in cylindrical tubes, Phys. Fluids **11**, 1890 (1999).

[13] V. V. Bychkov and M. A. Liberman, Dynamics and stability of premixed flames, Phys. Rep., **325**(4), 115 (2000).

[14] K. A. Kazakov, On-shell description of stationary flames, Phys. Fluids **17**, 032107 (2005).

[15] G. Joulin, H. El-Rabii, and K. A. Kazakov, On-shell description of unsteady flames, J. Fluid Mech. **608**, 217 (2008).

[16] G. I. Sivashinsky, Nonlinear analysis of hydrodynamic instability in laminar flames I. Derivation of basic equations, Acta Astronautica **4**(11), 1177 (1977).

[17] G. I. Sivashinsky and P. Clavin, On the nonlinear theory of hydrodynamic instability in flames, J. Phys. **48**, 193 (1987).

[18] G. Joulin and P. Cambray, On a tentative, approximate evolution equation for markedly wrinkled premixed flames, Combust. Sci. Technol. **81**, 243 (1992).

[19] J. Yanez and M. Kuznetsov, An analysis of flame instabilities for hydrogen-air mixtures based on Sivashinsky equation, Phys. Lett. A **380**, 2549 (2016).

[20] Y. Nomi, H. Gotoda, S. Kandani, and C. Almarcha, Complex network analysis of the gravity effect on premixed flames propagating in a hele-shaw cell, Phys. Rev. E **103**, 022218 (2021).

[21] D. M. Michelson and G. I. Sivashinsky, Nonlinear analysis of hydrodynamic instability in laminar flames. II. Numerical experiments, Acta Astronaut. **4**, 1207 (1977).

[22] D. M. Michelson and G. I. Sivashinsky, Thermal-expansion induced cellular flames, Combust. Flame **48**, 211 (1982).

[23] F. Creta, N. Fogla, and M. Matalon, Turbulent propagation of premixed flames in the presence of Darrieus-Landau instability, Combust. Theory Modell. **15**, 267 (2011).

[24] B. Denet, Sivashinsky equation in a rectangular domain, Phys. Rev. E **75**, 046310 (2007).

[25] G. Searby, J.-M. Truffaut, and G. Joulin, Comparison of experiments and a nonlinear model equation for spatially developing flame instability, Phys. Fluids **13**, 3270 (2001).

[26] C. Almarcha, B. Radisson, E. Al Sarraf, E. Villermaux, B. Denet, and J. Quinard, Interface dynamics, pole trajectories, and cell size statistics, Phys. Rev. E **98**, 030202(R) (2018).

[27] B. Radisson, B. Denet, and C. Almarcha, Nonlinear dynamics of premixed flames: From deterministic stages to stochastic influence, J. Fluid Mech. **903**, A17 (2020).

[28] P. Clavin and G. Searby, *Combustion Waves and Fronts in Flows: Flames, Shocks, Detonations, Ablation Fronts and Explosion of Stars* (Cambridge University, Cambridge, England, 2016).

[29] B. Denet, Intrinsic instabilities of curved premixed flames, Europhys. Lett. **21**, 299 (1993).

[30] B. Denet, On non-linear instabilities of cellular premixed flames, Combust. Sci. Technol. **92**, 123 (1993).

[31] B. Denet and J.-L. Bonino, Laminar premixed flame dynamics: A comparison of model and complete equations, Combust. Sci. Technol. **99**, 235 (1994).

[32] G. Boury, P. Cambray, and G. Joulin, Mean cell wavelengths of wrinkled premixed flames in weak gravity fields: Spontaneous evolutions, Combust. Theory Modell. **8**, 811 (2004).

[33] M. Tayyab, B. Radisson, C. Almarcha, B. Denet, and P. Boivin, Experimental and numerical Lattice-Boltzmann investigation of the Darrieus-Landau instability, Combust. Flame **221**, 103 (2020).

[34] B. Denet and P. Haldenwang, A numerical study of premixed flames Darrieus-Landau instability, Combust. Sci. Technol. **104**, 143 (1995).

[35] Y. Rastigejev and M. Matalon, Numerical simulation of flames as gas-dynamic discontinuities, Combust. Theory Modell. **10**, 459 (2006).

[36] C. Altantzis, C. E. Frouzakis, A. G. Tomboulides, M. Matalon, and K. Boulouchos, Hydrodynamic and thermodiffusive instability effects on the evolution of laminar planar lean premixed hydrogen flames, J. Fluid Mech. **700**, 329 (2012).

[37] N. Fogla, F. Creta, and M. Matalon, Effect of folds and pockets on the topology and propagation of premixed turbulent flames, Combust. Flame **162**, 2758 (2015).

[38] R. Yu, X.-S. Bai, and V. Bychkov, Fractal flame structure due to the hydrodynamic Darrieus-Landau instability, Phys. Rev. E **92**, 063028 (2015).

[39] A. Patyal and M. Matalon, Nonlinear development of hydrodynamically-unstable flames in three-dimensional laminar flows, Combust. Flame **195**, 128 (2018).

[40] Z. Rakib and G. I. Sivashinsky, Instabilities in upward propagating flames, Combust. Sci. Technol. **54**, 69 (1987).

[41] G. Boury, Etudes Théoriques et Numériques de Fronts de Flammes Plissées: Dynamiques Non-Linéaires Libres Ou Bruitées, Ph.D. thesis, Université de Poitiers, 2003.

[42] F. Veiga-López, M. Kuznetsov, D. Martínez-Ruiz, E. Fernández-Tarrazo, J. Grune, and M. Sánchez-Sanz, Unexpected Propagation of Ultra-Lean Hydrogen Flames in Narrow Gaps, Phys. Rev. Lett. **124**, 174501 (2020).

[43] K. A. Kazakov, Premixed flame propagation in vertical tubes, Phys. Fluids **28**, 042103 (2016).

[44] E. Al Sarraf, C. Almarcha, J. Quinard, B. Radisson, B. Denet, and P. Garcia-Ybarra, Darrieus-Landau instability and Markstein numbers of premixed flames in a Hele-Shaw cell, Proc. Combust. Inst. **37**, 1783 (2019).

[45] B. Radisson, J. Piketty-Moine, and C. Almarcha, Coupling of vibro-acoustic waves with premixed flame, Phys. Rev. Fluids **4**, 121201(R) (2019).

[46] L. Berger, K. Kleinheinz, A. Attili, and H. Pitsch, Characteristic patterns of thermodiffusively unstable premixed lean hydrogen flames, Proc. Combust. Inst. **37**, 1879 (2019).

[47] D. Martínez-Ruiz, F. Veiga-López, D. Fernández-Galisteo, V. N. Kurdyumov, and M. Sánchez-Sanz, The role of conductive heat losses on the formation of isolated flame cells in hele-shaw chambers, Combust. Flame **209**, 187 (2019).

[48] D. Vaynblat and M. Matalon, Stability of pole solutions for planar propagating flames. I. Exact eigenvalues and eigenfunctions, SIAM J. Appl. Math. **60**, 679 (2000).

[49] D. Vaynblat and M. Matalon, Stability of pole solutions for planar propagating flames. II. Properties of eigenvalues/eigenfunctions and implications to stability, SIAM J. Appl. Math. **60**, 703 (2000).

[50] O. Thual, U. Frisch, and M. Hénon, Application of pole decomposition to an equation governing the dynamics of wrinkled flame fronts, J. Phys. **46**, 1485 (1985).

[51] D. G. Goodwin, H. K. Moffat, and R. L. Speth, Cantera: An object-oriented software toolkit for chemical kinetics, thermodynamics, and transport processes, version 2.3.0, 2017, arXiv:10.5281/zenodo.170284.

[52] S. D. Mechanism, Chemical-kinetic mechanisms for combustion applications, http://combustion.ucsd.edu (2016).